Supplemental Data

Supplemental Table 1: Chromosome 6p25 SNPs associated with WMH and *FOXC1* transcript levels.

SNP	*P*-value GWA	Corrected *P*-value* GWA	*P*-value eQTL[1]	Z-score eQTL[1]	*P*-value eQTL[2]	Z-score eQTL[2]
rs12206258	6.44×10^{-5}	0.0031	5.82×10^{-11}	-6.55	0.008	-3.45
rs12203614	9.36×10^{-5}	0.0046	--	--	--	--
rs12199578	0.000117	0.0056	--	--	--	--
rs12193217	0.000116	0.0056	--	--	--	--
rs10458129	0.000546	0.026	--	--	--	--
rs12206340	0.000614	0.029	--	--	--	--
rs12189662	0.000616	0.030	--	--	--	--
rs6936881	0.000684	0.033	2.96×10^{-8}	-5.54	0.01	-3.03
rs7765461	0.000892	0.043	--	--	--	--
rs7765344	0.001002	0.048	2.64×10^{-8}	-5.56	0.01	-3.03

* Correction based on 48 linkage disequilibrium blocks in the region analyzed
[1] Westra HJ et al. (2013) [2] Fu J et al. (2012)
GWA: Genome wide association eQTL: Expression quantitative trait loci

Supplemental Table 2: MRI data from patients with *FOXC1* mutations or copy number variants

Age	Genotype	Affected Gene(s)	MRI Phenotype	Images
50[a]	Ser82Thr	*FOXC1*	WMH	S1B
04[a]	Ser82Thr	*FOXC1*	WMH, MCM, CVH	1D/S1C
60[a]	Ser82Thr	*FOXC1*	WMH	S1D
55[b]	Ser131Leu	*FOXC1*	WMH, DPVS	1C
31[g]	Pro274fs	*FOXC1*	DPVS	--
05[g]	Pro274fs	*FOXC1*	WMH, DPVS	1E
60[h]	Gly34fs	*FOXC1*	WMH	1F
33[c]	6p25 Del.	*FOXC1, FOXF2*	WMH, DPVS, MCM	--
02[c]	6p25 Del.	*FOXC1, FOXF2*	WMH, DPVS, MCM, CVH	1G
15[d]	6p25 Del.	*FOXC1*	DPVS	--
17[d]	6p25 Del.	*FOXC1*	DPVS	--
01[e]	6p25 Del.	*FOXC1, GMDS, C6ORF195, MYLK4*	WMH, MCM	--
14[f]	6p25 Dup.	*FOXC1, FOXF2, GMDS*	Lacunar infarct	1H
42[f]	6p25 Dup.	*FOXC1, FOXF2, GMDS*	DPVS	--
48[f]	6p25 Dup.	*FOXC1, FOXF2, GMDS*	WMH, DPVS	--
85[f]	6p25 Dup.	*FOXC1, FOXF2, GMDS*	WMH, DPVS	--
79[f]	6p25 Dup.	*FOXC1, FOXF2, GMDS*	DPVS, Aneurysm	--
28[g]	6p25 Dup.	*FOXC1, FOXF2, GMDS*	DPVS	--

WMH: White matter hyperintensities
DPVS: Dilated perivascular spaces
MCM: Mega cisterna magna
CVH: Cerebellar vermis hypoplasia
Identical genotypes by descent are denoted by the same superscript.

Supplemental Table 3: Quantification of cerebral hemorrhage prevalence induced by manipulating *foxc1* or *pdgfr*.

Treatment Applied	Number of Embryos with Cerebral Hemorrhage	Number of Treated Embryos	Cerebral Hemorrhage Prevalence (%)
foxc1a MO 2ng *foxc1b* MO 2ng	111	352	31.5
foxc1a MM MO 2ng *foxc1b* MM MO 2ng	21	277	7.6
foxc1a mRNA 75 pg	32	111	28.8
pdgfra MO 8ng	32	170	18.8
pdgfrb MO 8ng	6	134	4.5
pdgfra MO 4ng *pdgfrb* MO 4ng	34	117	29.1
Crenolanib (10uM)	38	79	48.1

MO: morpholino oligonucleotide, MM MO: 5 base pair mis-match morpholino oligonucleotide

Supplemental Table 4: SNPs near *PITX2* are associated with WMH

SNP	*P*-value	Corrected *P*-value*
rs2129979	0.0005498	0.0071
rs11931959	0.0005594	0.0073
rs13121924	0.001578	0.021
rs3866831	0.001605	0.021
rs6533531	0.001621	0.021
rs3866832	0.001635	0.021
rs13141190	0.001640	0.021
rs6533530	0.001644	0.021
rs7697491	0.001661	0.022
rs723363	0.001674	0.022

***** Correction based on 13 linkage disequilibrium blocks in the region analyzed

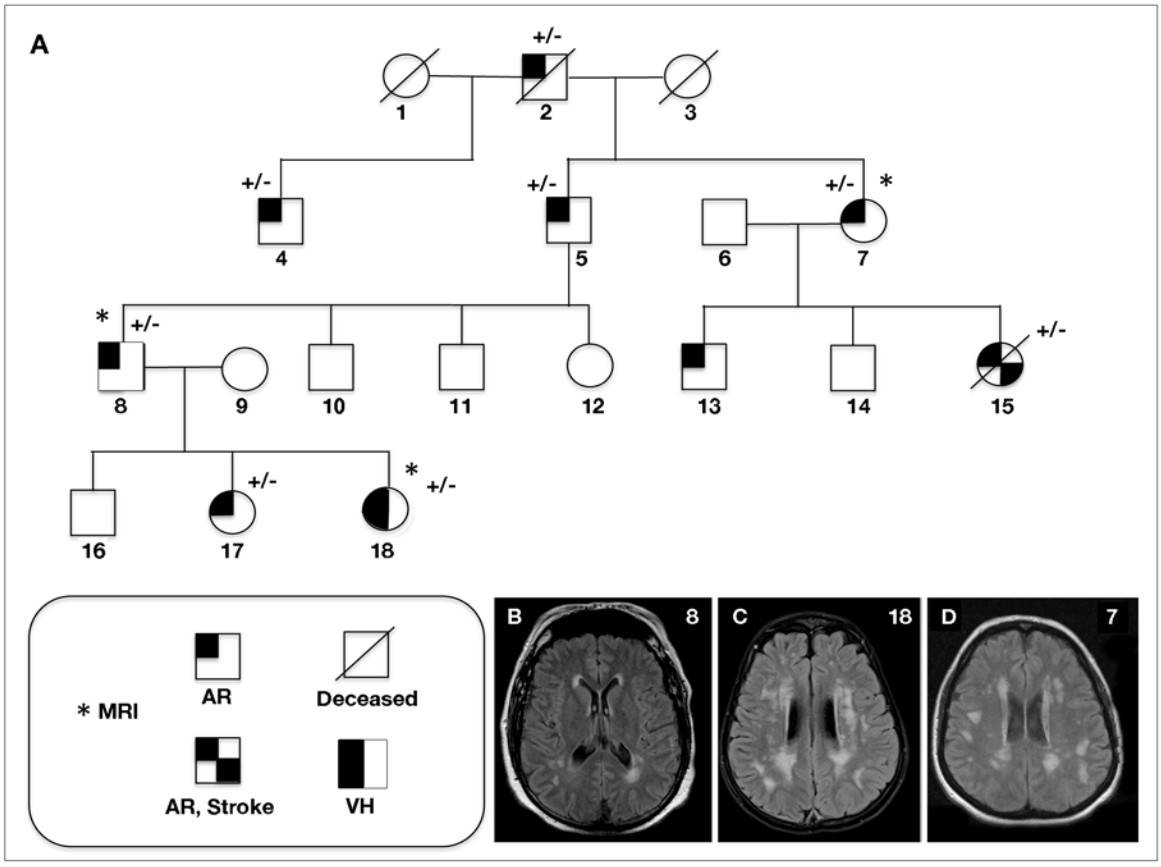

Supplemental Figure 1: (**A**), Pedigree illustrating segregation of the *FOXC1* Ser82Thr mutation with Axenfeld-Rieger Syndrome and CSVD. (**B-D**), Axial FLAIR MRI (individuals #8, 18, and 7) demonstrates abundant white matter hyperintensities. Individual #18 had repeated hospitalizations for vascular hemiparesis (VH) between the ages of 4 and 8; individual #15 is deceased from a stroke aged 23 years.

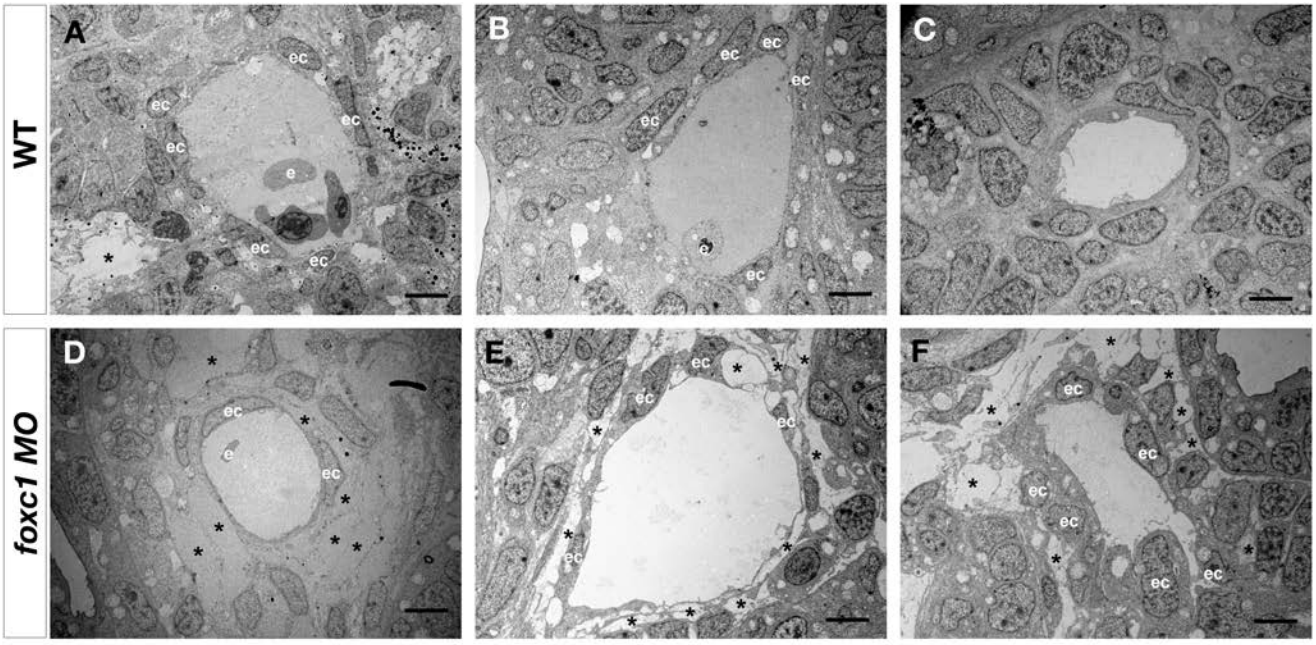

Supplemental Figure 2: Transmission electron micrographs of cerebral vessels at 52hpf demonstrate increased perivascular spaces in cross sections at the level of the hindbrain in *foxc1* morphants. Asterisks denote acellular areas adjacent to endothelial cells, suggesting detachment of vessels from surrounding cells. [Dorsal aorta (**A** and **D**), Pharyngeal arch artery (**B**, **C**, **E**, **F**); Endothelial cells (ec), Erythrocytes (e); Scale bars represent 2 μm].

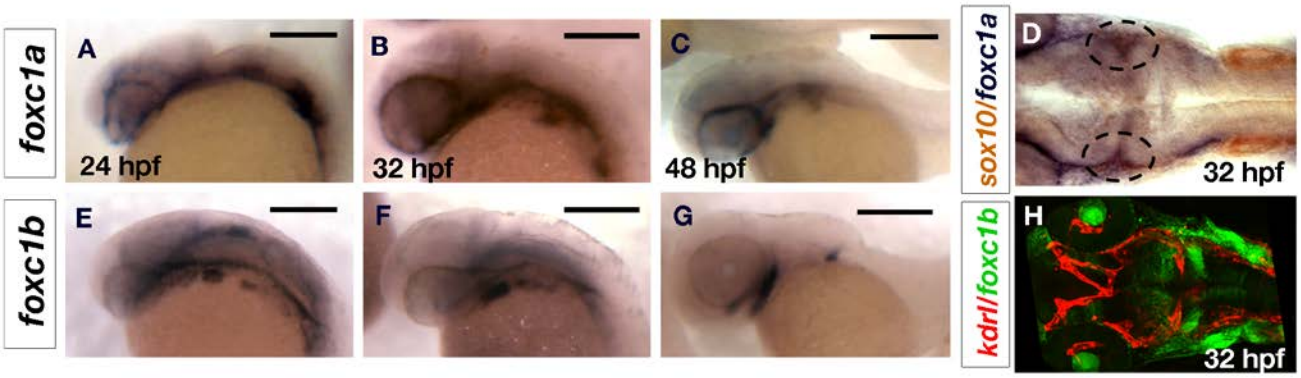

Supplemental Figure 3: Expression of *foxc1a* and *foxc1b* in the zebrafish neural crest. At early developmental stages, both *foxc1a* and *foxc1b* are expressed in neural crest populations (**A**, **B**, **E**, **F**). For *foxc1a*, this expression domain overlaps with the neural crest marker *sox10* at the mid-hindbrain boundary (**D**, dotted circles). At later stages, *foxc1a* and *foxc1b* expression is observed in structures heavily populated with neural crest cells such as the pharyngeal arches (**C**, **G**). Notably, expression of *foxc1b* is not observed in the developing endothelium, defined by *kdrl:mcherry* expression (**J**). [Scale bars 200μm; Magnification (**D**, **H**) 200X].

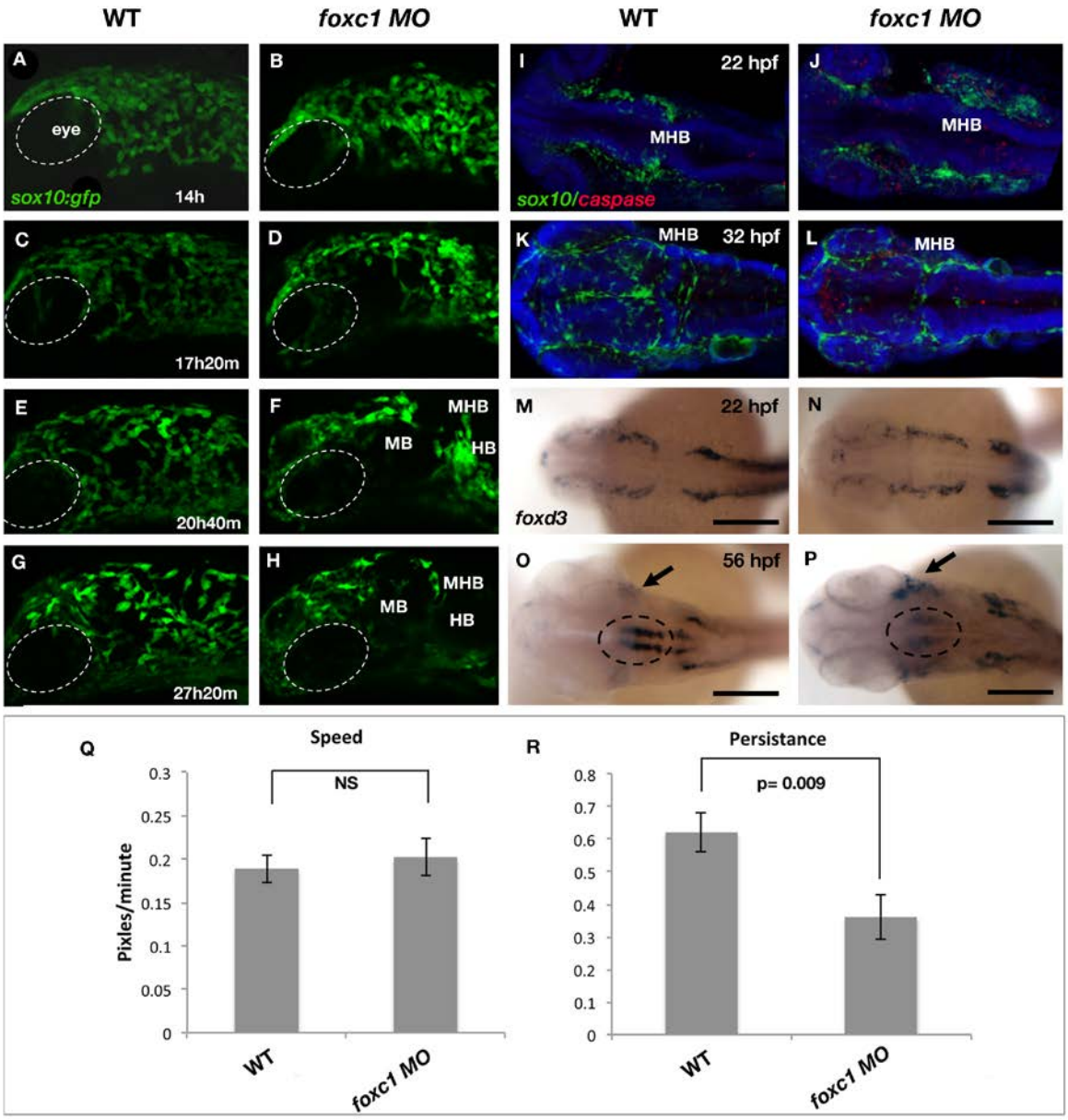
WT
foxc1 MO
WT
foxc1 MO
A
eye
sox10:gfp
14h
B
I
22 hpf
MHB
sox10/caspase
J
MHB
C
17h20m
D
K
MHB
32 hpf
L
MHB
E
20h40m
F
MHB
MB
HB
M
22 hpf
foxd3
N
G
27h20m
H
MHB
MB
HB
O
56 hpf
P
Q
Speed
NS
Pixles/minute
0.3
0.25
0.2
0.15
0.1
0.05
0
WT
foxc1 MO
R
Persistance
p= 0.009
0.8
0.7
0.6
0.5
0.4
0.3
0.2
0.1
0
WT
foxc1 MO

Supplemental Figure 4: Aberrant migration of neural crest cells in *foxc1* morphants. Live imaging demonstrates similar numbers of *sox10* positive neural crest cells at 14 hpf in wildtype (**A**), and *foxc1* morphants (**B**). However, in morphants, fewer neural crest cells are observed in the midbrain (MB), hindbrain (HB) and at the mid-hindbrain boundary (MHB) as development proceeds (**C**-**H**). Analysis of fixed tissues demonstrates delayed anterior migration of neural crest cells (**I**, **J**). There is moderately increased apoptosis in *foxc1* morphants, however this does not appear to be specific to the neural crest since it does not colocalize with *sox10* expression (**I**-**L**). Examination of *foxd3*, a second marker for neural crest, demonstrates delayed neural crest cell migration by 56 hpf. There are similar levels of neural crest cells in the brain periphery at 22hpf (**M**, **N**), and the majority of these cells migrate from the periphery (arrow) to the midline (dotted circle) by 56hpf in wildtype embryos (**O**). In contrast, in *foxc1* morphants, the majority of these foxd3 positive cells remain in the brain periphery (**P**). Although quantification reveals no alteration to the speed of *sox10* neural crest cell migration in *foxc1* morphants (**Q**), there is a significant difference in persistence (cell displacement/distance travelled), demonstrating an indirect migration course (**R**). [Magnification: 200X (**A**-**L**); Scale bars: 200μm].

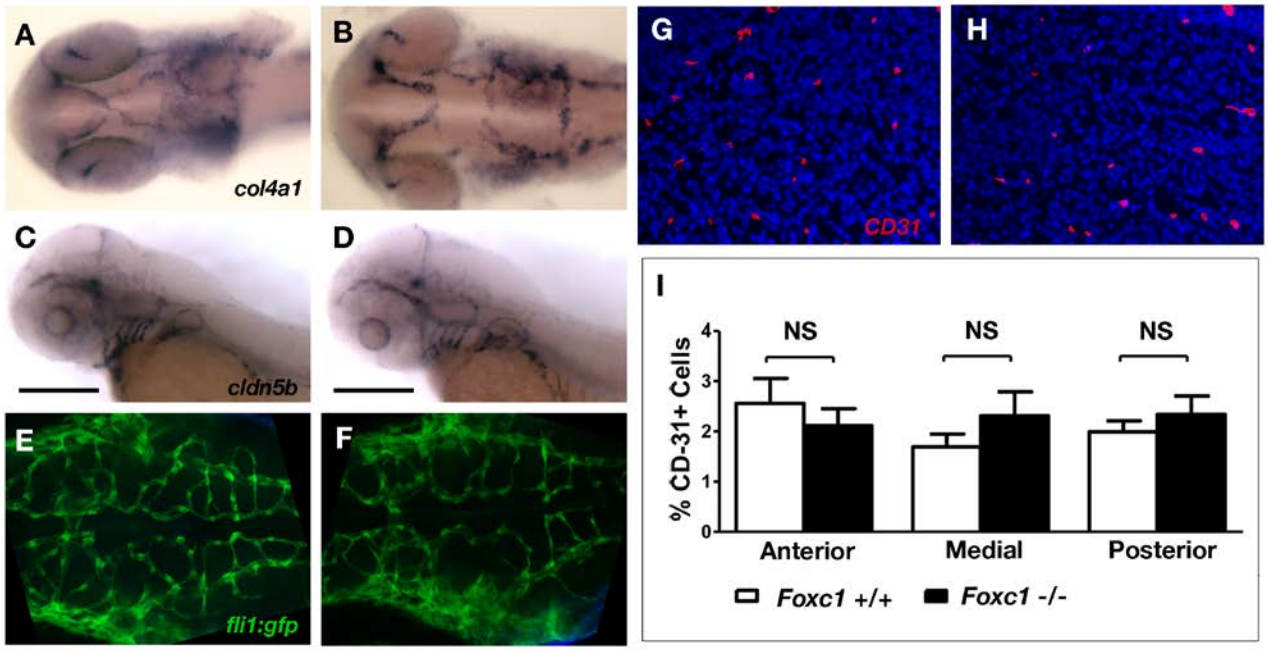

Supplemental Figure 5: Endothelial cell and vascular basement membrane marker expression is unaltered in *foxc1* morphants. Expression of *collagen 4a1* in the vascular basement membrane (**A**) is unchanged in *foxc1* morphants at 24 hpf (**B**), as is endothelial expression of tight junction marker *claudin 5b* at 72hpf (**C**) [morphants (**D**)]. Visualization of endothelial cells [*fli1:gfp* reporter] reveals no difference in vessel formation or morphology between WT (**E**) and *foxc1* morphants (**F**). Similarly, analysis of endothelial (CD31+) cell density reveals no difference between wildtype (**G**) and murine mutants with endothelial specific loss of *Foxc1* (**H**) [Quantification of endothelial cell density (**I)**]. [Magnification: 200X (**A**, **B**, **G**, **H**), 400X (**E**, **F**); Scale bars: 200μm].

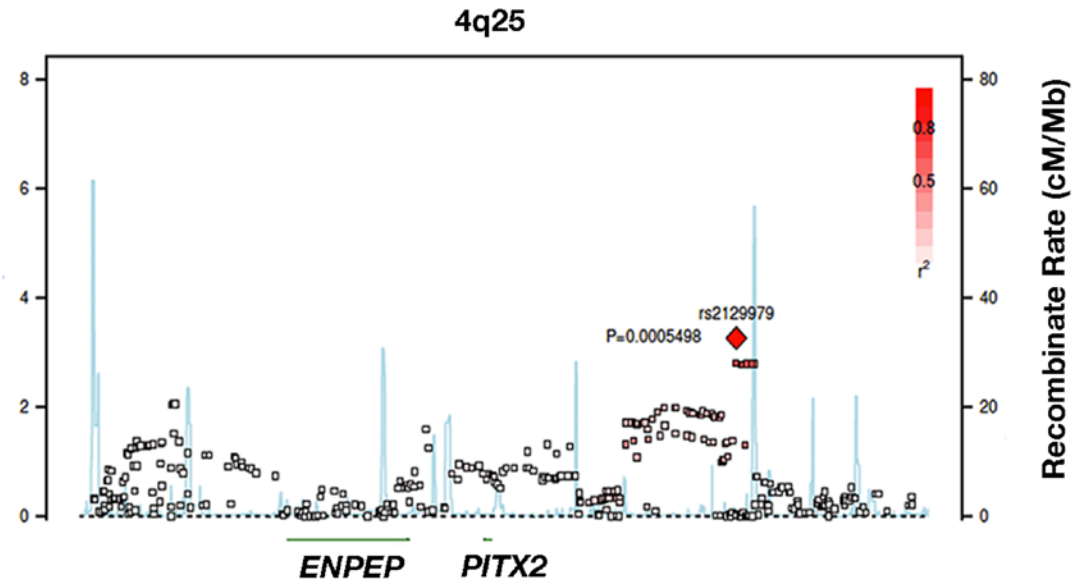

Supplemental Figure 6: Association of SNPs located near *PITX2* on 4q25 with white matter hyperintensities [Meta-analysis, CHARGE Consortium]. 10 SNPs, located 5' to the *PITX2* coding sequence remain significant after a modified Bonferroni correction for the number of disequilibrium blocks (13) in the region.

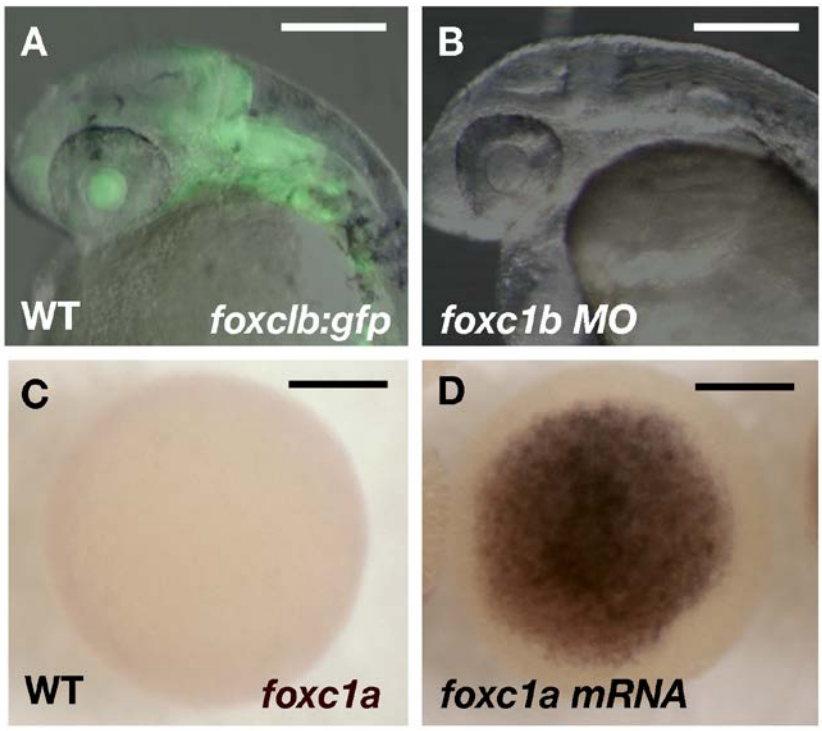

Supplemental Figure 7: (**A, B**) The effectiveness of the *foxc1b* translation blocking morpholino is demonstrated via the abrogation of *gfp* driven by the *foxc1b* promoter (containing the morpholino binding sequence). (**C, D**) Injection of 75 pg of *foxc1a* mRNA results in a vast increase in message, detected by in situ hybridization at 50% epiboly. [Scale bars: 200μm].

Supplemental Methods

Meta-Analysis of Genome wide association data and eQTL analysis

A meta-analysis was conducted on SNP data from the CHARGE Consortium, comprising more than 9361 stroke-free individuals with MRIs, derived from community-based cohorts of European descent. The data is graphically presented as -Log *P*-value, with a Bonferroni correction for the number of independent comparisons [determined via the number of linkage disequilibrium blocks (Life Technologies SNP browser V3.1 software)]. Expression QTL analysis was performed, using data from two independent studies. The first, contained 5311 blood samples from which transcript levels were determined (http://genenetwork.nl/bloodeqtlbrowser/) (1), while the second comprised 1536 blood and tissue samples (2).

Patient recruitment and magnetic resonance imaging

18 patients with Axenfeld-Rieger Syndrome due to *FOXC1* mutation or CNV were recruited for research MRIs from a previously collected cohort. Additional clinical MRIs were obtained from regional imaging centers, with the earliest imaging time point being one year of age. MRIs included Axial-T1 and T2 weighted images, fluid attenuation inversion recovery (FLAIR) and gradient echo (GRE) sequences. All MRIs shown are FLAIR sequences (except a T2-weighted spin echo sequence, Fig. 3H). All MRIs were assessed by a board-certified neuroradiologist.

Molecular analysis of the Axenfeld-Rieger Cohort

The 18 Axenfeld-Rieger patients were previously demonstrated by Sanger sequencing and copy number analysis to have *FOXC1*-attributable disease. The missense mutations (Ser82Thr and Ser131Leu) alter invariant residues in the conserved forkhead domain and have reduced functionality (3), while the two frameshift mutations are anticipated to be either nulls or strong hypomorphs. The

first (Gly34fs) truncates the protein prior to the forkhead domain, abrogating DNA binding, while the second (Pro274fs) results in loss of over half the amino acid sequence including residues required for transcriptional co-activation (4). The breakpoints of each CNV have been defined (5) and these result in deletion of *FOXC1* alone, or deletion/duplication of *FOXC1* and adjacent genes on 6p25 including *FOXF2, GMDS, C6ORF195* and *MYLK4* (Supplemental Table 2).

Zebrafish injections and interaction experiments

Since there are two paralogs (*foxc1a* and *foxc1b*), reflecting teleost's ancestral genome duplication, both were inhibited with previously reported morpholino oligonucleotides [*foxc1a*^{MO}: CCTGCAT-GACTGCTCTCCAAAACGG, *foxc1b*^{MO}: GCATCGTACCCCTTTCTTCGGTACA] (6). All data are from one-cell stage embryos injected with 2ng of *foxc1a*^{MO} and 2ng of *foxc1b*^{MO}, unless otherwise noted. As one control for specificity, injection of equal amounts of 5-base pair mis-matched morpholinos were utilized [*foxc1a*: CTTGCCTGAATGCTCTCTAAAACGT, *foxc1b*: GCAGCGTA-CGCATTTCTACGGTCCA]. The effectiveness of the active *foxc1b*^{MO} is evident from the loss of *foxc1b:gfp* translation (Supplemental Figure 7A, B). For overexpression, *foxc1a* cDNA was cloned into pCS2+, sense mRNA transcribed, and 75pg mRNA injected into zebrafish one cell embryos. This resulted in a profound increase in *foxc1a* message on in situ hybridization **(**Supplemental Figure 7C, D). Previously published morpholinos, with demonstrated effectiveness and specificity, were used to inhibit *pdgfra* and *pdgfrb* function (7, 8).

For the interaction experiments, the sub-optimal dose of each morpholino or morpholino combination was determined by assaying the prevalence of cerebral hemorrhage induced [1ng *foxc1a*^{MO} and 1ng *foxc1b*^{MO}; 4ng *pdgfra*^{MO} alone; 4ng *pdgfrb*^{MO} alone; 2ng *pdgfra*^{MO} and 2ng *pdgfrb*^{MO}]. The pan-*pdgfr* inhibitor, Crenolanib, was used at 10μM, and at 1 μM for sub-optimal inhibition. Student *t*-tests were

used to determine if sub-optimal inhibition of both Pdgfr signaling and *foxc1* increased the prevalence of cerebral hemorrhage compared to sub-optimal inhibition of *foxc1* alone.

Zebrafish Imaging and immunohistochemistry

For in situ hybridization, embryos were fixed overnight in 4% paraformaldehyde (PFA), permeabilized (10μg/ml Proteinase K) and hybridized overnight at 65°C. Transgenic lines (*foxc1b:gfp*, *kdrl:gfp*^{la116}, *acta:gfp*^{ca7}*/kdrl:mcherry*^{ci5}) were mounted in AquaMount (Polysciences Inc) or low melt agrose and confocal imaged using 10x or 20x (dry) or 40x (oil immersion) objectives. For live imaging, *sox10:gfp* embryos were mounted laterally in low melting point agrose, and z-stack images captured every 10 minutes for 24 hours. For analysis of apoptosis, after fixation (4% PFA) and permeabilization (10μg/ml Proteinase K), goat anti-rabbit activated Caspase 3 (BMD Biosciences) was used (1/1000 dilution in 5% goat serum) and detected using Alexa Fluor568 (Life Technologies).

Quantification of cell number and migration

Sox10:egfp and *kdrl:mcherry* transgenic zebrafish lines were crossed to permit visualization of neural crest cells (*sox10*) and blood vessel endothelium (*kdrl*), allowing the number of *sox10* positive neural crest cells contacting cerebral blood vessels to be quantified. The number of vessel contacting eGFP positive cells were normalized per 50 μm length of blood vessel (from 11 wildtype and 14 *foxc1* morphant embryos at 32 hpf). For analysis of the speed (pixels travelled/time) and persistence (cell displacement/total distance travelled) of neural crest cell migration, cell trajectories were computed using ImageJ (particle tracker plugin) for 15 wildtype and 15 *foxc1* morphant neural crest cells. To quantify vascular smooth muscle cell number at 4 dpf, cells expressing *acta2:gfp* were manually counted for 12 wildtype and 11 *foxc1* morphant embryos. All discrete GFP positive cells in the ventral

head vasculature (pharyngeal arches and jaw) as well as the cardiac outflow tract were counted. Researchers were masked as to the genotype for all cell-counting assays.

Zebrafish foxc1b reporter line

This reporter line was kindly provided by Dr. Brain Link (Medical College of Wisconsin, Milwaukee) and had been generated in his laboratory as follows. A 5 kb fragment from the *foxc1b* ATG start codon was coned into a 5' gateway entry vector. Recombination reactions using LR clonase were performed to create *pDESTTol2: -5.0foxc1b:EGFP:polyA*, which was injected into zebrafish one cell embryos with *tol2* mRNA. F0 embryos were screened for mosaic EGFP expression. The mw44 insertion was chosen due to similarity in *foxc1b* expression, and outcrossed to create the F2 generation [*Tg(-5.0foxC1b:EGFP)mw44*].

Mouse Immunohistochemistry

Murine cerebral vasculature was analyzed by CD-31 immunostaining of the midbrain at E15.5, in four embryos for each genotype (*EC-Foxc1*$^{-/-}$ and *Foxc1*$^{F/F}$). Sections were blocked in 10% donkey serum for 30 minutes, stained overnight at 4 °C using a 1:50 dilution of Rat anti-CD-31 (BD Biosciences), and then for one hour at room-temperature using a 1:250 dilution of Alexa Fluor647 anti-Rat (Life Technologies). After washing, sections were DAPI counterstained and mounted using VECTASHIELD mounting media (Vector Laboratories). All images were taken at 20X magnification on either a Zeiss Axio Observer.D1 or an AMG EVOS.FL fluorescent microscope.

Image analysis was completed with the use of ImageJ software (NIH), utilizing the *analyze particles* function. Researchers remained masked to genotypes of all samples. For statistical analysis, 12-13 images were quantified per group. For each brain region, the mean CD-31+ cell density was calculated

and compared across genotypes. The Standard Error of the Mean (SEM) was calculated for each group and represented through the use of error bars. An unpaired, two-tailed Student's t-test was used to compare genotypes at each brain region. Amongst the three mid-brain regions analyzed, no p-value reached lower than 0.25, indicating no statistical significance in any data-sets analyzed.

For analysis of E15.5 *Pitx2*$^{-/-}$ mice, tissues were fixed in 4% PFA, washed, and embedded in paraffin. Longitudinal sections (6-8μm) were cut, de-waxed in xylene, and rehydrated; with four embryos analyzed [wildtype (n=2), *Pitx2*$^{-/-}$ (n=2)]. The smooth muscle actin epitope was exposed by boiling in 10mM citric acid, then an anti-alpha smooth muscle Actin antibody (Abcam) was used with AlexaFluor 488 (Life Sciences) and DAPI nuclear stain to visualize vascular smooth muscle. After imaging at 40x on a Zeiss LSM 700 confocal microscope, 8 sections from each mouse were analyzed, with quantification performed on a total of 10 sections from each genotype.

Transmission electron microscopy

Transmission electron microscopy was performed as previously described (9), with a minimum of 4 vessels analyzed in each embryo (4 wildtype and 4 *foxc1* morphants).

References for Supplemental Methods

1. Westra, H.J., Peters, M.J., Esko, T., Yaghootkar, H., Schurmann, C., Kettunen, J., Christiansen, M.W., Fairfax, B.P., Schramm, K., Powell, J.E., et al. 2013. Systematic identification of trans eQTLs as putative drivers of known disease associations. *Nat Genet* 45:1238-1243.
2. Fu, J., Wolfs, M.G., Deelen, P., Westra, H.J., Fehrmann, R.S., Te Meerman, G.J., Buurman, W.A., Rensen, S.S., Groen, H.J., Weersma, R.K., et al. 2012. Unraveling the regulatory mechanisms underlying tissue-dependent genetic variation of gene expression. *PLoS Genet* 8:e1002431.
3. Saleem, R.A., Banerjee-Basu, S., Berry, F.B., Baxevanis, A.D., and Walter, M.A. 2001. Analyses of the effects that disease-causing missense mutations have on the structure and function of the winged-helix protein FOXC1. *Am J Hum Genet* 68:627-641.
4. Berry, F.B., Lines, M.A., Oas, J.M., Footz, T., Underhill, D.A., Gage, P.J., and Walter, M.A. 2006. Functional interactions between FOXC1 and PITX2 underlie the sensitivity to FOXC1 gene dose in Axenfeld-Rieger syndrome and anterior segment dysgenesis. *Hum Mol Genet* 15:905-919.
5. Chanda, B., Asai-Coakwell, M., Ye, M., Mungall, A.J., Barrow, M., Dobyns, W.B., Behesti, H., Sowden, J.C., Carter, N.P., Walter, M.A., et al. 2008. A novel mechanistic spectrum underlies glaucoma-associated chromosome 6p25 copy number variation. *Hum Mol Genet* 17:3446-3458.
6. Skarie, J.M., and Link, B.A. 2009. FoxC1 is essential for vascular basement membrane integrity and hyaloid vessel morphogenesis. *Invest Ophthalmol Vis Sci* 50:5026-5034.
7. Wiens, K.M., Lee, H.L., Shimada, H., Metcalf, A.E., Chao, M.Y., and Lien, C.L. 2010. Platelet-derived growth factor receptor beta is critical for zebrafish intersegmental vessel formation. *PLoS One* 5:e11324.
8. Kartopawiro, J., Bower, N.I., Karnezis, T., Kazenwadel, J., Betterman, K.L., Lesieur, E., Koltowska, K., Astin, J., Crosier, P., Vermeren, S., et al. 2014. Arap3 is dysregulated in a mouse model of hypotrichosis-lymphedema-telangiectasia and regulates lymphatic vascular development. *Hum Mol Genet* 23:1286-1297.
9. Liu, J., Fraser, S.D., Faloon, P.W., Rollins, E.L., Vom Berg, J., Starovic-Subota, O., Laliberte, A.L., Chen, J.N., Serluca, F.C., and Childs, S.J. 2007. A betaPix Pak2a signaling pathway regulates cerebral vascular stability in zebrafish. *Proc Natl Acad Sci U S A* 104:13990-13995.